

Tunneling of Micro-sized Droplets Through a Flowing Soap Film

Ildoo Kim and X.L. Wu

Department of Physics and Astronomy,

University of Pittsburgh, Pittsburgh, PA 15260

(Dated: March 26, 2010)

Abstract

When a micron-sized water droplet impacts on a freely suspended soap film with speed v_i , there exists a critical impact velocity of penetration v_C . For the droplet with $v_i < v_C$, it flows with the soap film after the impact whereas with $v_i > v_C$, it tunnels through. In all cases, the film remains intact despite the fact that the droplet radius ($R_0 = 26 \mu\text{m}$) is much greater than the film thickness ($0 < h \lesssim 10 \mu\text{m}$). The critical velocity v_C was measured as a function of h , and interestingly v_C approaches an asymptotic value $v_{C0} \simeq 520 \text{ cm/s}$ in the limit $h \rightarrow 0$. This indicates that in addition to an inertial effect, a deformation or stretching energy of the film is required for penetration. Quantitatively, we found that this deformation energy corresponds to the creation of ~ 14 times of the cross-sectional area of the droplet ($14\pi R_0^2$) or a critical Weber number $We_C (\equiv 2R_0\rho_w v_{C0}^2/\sigma) \simeq 44$, where ρ_w and σ are respectively the density and the surface tension of water.

PACS numbers: 47.55.D-, 47.55.dr, 47.15.gm

I. INTRODUCTION

When a liquid droplet impinges on a surface made of the same liquid, a variety of phenomena occurs. If the underlying liquid has a finite but large depth, the droplet causes splashing, creating a crown-like structure that had become an iconic piece of Edgerton's then newly invented strobe photography in the late 30's [1]. If the underlying liquid has a small thickness, the macroscopic corona structure disappears altogether and instead a thin ejecta sheet is created [2]. The existence of such ejecta sheet has only recently been discovered and has captured the attention of scientists [3]. Underlying this seemingly simple phenomenon is complex dynamics [3–5], whose understanding is currently incomplete but is fundamentally important for a variety of industrial processes such as containment of hazardous liquids, uniform coating of surfaces, and efficient fuel injection.

In this paper, we report a related subject, namely the impact of a water droplet against a freely flowing soap film. Specifically, we are interested in the condition of tunneling of a ballistic droplet through the film. A classical analysis of Taylor and Michael [6] based on an energy argument suggests that when a hole is created on a liquid film, it will shrink and heal if its diameter is smaller than the film thickness. On the other hand, if the diameter is larger than the thickness, an instability that leads to the rupture of the film will occur. Analyses were also carried out by Zheng and Witten [7] in a proposal to create a giant liquid film in space that is free of gravitational forces and surrounding air; both are significant factors complicating the study of two-dimensional fluid flows and turbulence using these films in an earth environment [8–10]. Their calculation shows that a meteor of a few nanometer in size can be hazardous to a space-based film. While the energetic argument is compelling and has found some experimental confirmations [11], the calculation cannot account for certain observations made in these films. For instance, common experiences show that when a soap film is perturbed by a foreign object, the film often breaks. However, if the object is wetted by water, the film is much more resistant to the perturbation. A recent experiment demonstrated that a macroscopic object as large as a tennis ball can readily pass through a micron-thick film without breaking it [12]. It is evident that the passage dynamics in this latter case cannot be understood unless film deformation into the third dimension, perpendicular to the film, is taken into account.

To investigate the tunneling process quantitatively we implemented an inkjet technique to

generate uniform sized ($R_0 = 26\ \mu\text{m}$) water droplets at a controllable rate. The trajectories of the droplets before and after impacts are digitized using a high-speed video camera, allowing quantitative measurements of momentum and energy transfers between the droplets and the film. It was observed that droplets can tunnel through the soap film if its impact velocity is higher than a certain threshold value v_C , and in no case rupture occurs as a result of the impact. Using films of different thicknesses ($0 < h \lesssim 10\ \mu\text{m}$), we found that the energy barrier $E_C = \frac{1}{2}mv_C^2$ for tunneling is a linear function of h and can be expressed as $E_C = E_{min}(1 + \alpha h/R_0)$, where $E_{min} \simeq 0.01\ \text{erg}$ and $\alpha \simeq 3.9$ are constants. Kinematically, we found that the tunneling process can be modeled as an inelastic collision between the droplet and the film. It only requires two parameters, M_1 and M_2 , which specify respectively the effective mass of the film involved in the collision and the mass that is transferred to the droplet after the collision.

II. EXPERIMENTAL SETUP

Our experiment was carried out in a vertically flowing soap film as depicted in Fig. 1. The construction of the soap-film apparatus has been discussed previously [13, 14]. Briefly, our soap-film channel is made of two parallel nylon wires, which are connected to two soap solution reservoirs, one at the top and the other at the bottom of the channel. To create a soap film, we first let the soap solution flow along the two wires, and then the wires are separated from each other to form a film. The channel width in the current measurement is set constant at 5 cm. The soap solution collected by the lower reservoir is pumped back to the top reservoir, resulting in a long-lasting film once it is initiated. The film flow speed ($1.5 < V_F < 2.5\ \text{m/s}$) and the thickness ($0 < h \lesssim 10\ \mu\text{m}$) can be varied by regulating the solution flux by a valve at the injection point at the top of the channel.

The soap solution used consists of 2% (in volume) liquid detergent (Dawn) and 98% distilled water. The kinematic viscosity of the soap solution, measured by a glass capillary viscometer (Cannon Instrument Co.), is $\nu \simeq 0.012\ \text{cm}^2/\text{s}$, close to water. The surface tension of the liquid/air interface of the bulk solution was determined by a Du Noüy tensiometer (CSC Scientific) as $\sigma \simeq 32 \pm 1\ \text{erg/cm}^2$. Measurements of σ as a function of the concentration of the liquid detergent indicate that the critical micellar concentration of our soap solution is well below 0.1%. As will be discussed below, a wave speed measurement in the soap film

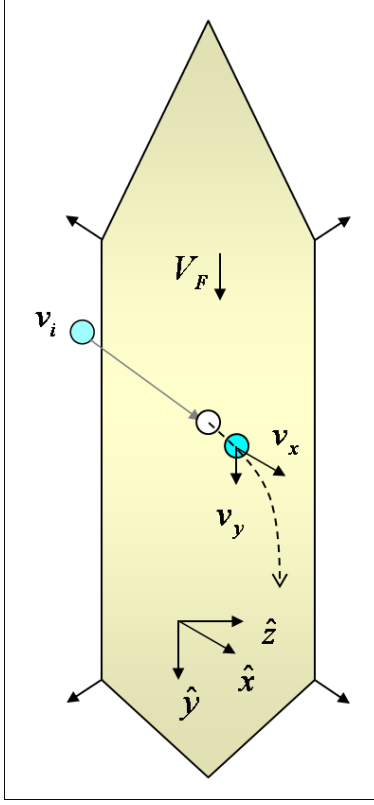


Figure 1: The experimental setup. A vertical soap film flows in the \hat{y} direction with a uniform velocity V_F . A water droplet is ejected horizontally, in the \hat{x} direction, toward the soap film with an impact velocity v_i . The final velocity of the droplet after impact (v_x, v_y) is also indicated. To visualize the water droplet and the film, a high-intensity halogen lamp and a low-pressure sodium lamp were used. The droplet's trajectories and their corresponding velocities were recorded by a high-speed video camera.

indicates that the surface tension of the film is about the same as measured on the free surface of the bulk liquid, indicating that at 2% concentration, the surfaces of the film are fully covered by the surfactant.

Micron-sized water droplets are created by using an inkjet printer cartridge (NEC model #30-060). This cartridge works by electrically heating water near a nozzle, which consists of a small heater with a $30\ \Omega$ internal resistance. When a pulse of electric current is applied, the rapid expansion of water near the heater causes a droplet to be ejected with a high speed. By using a custom-made computer program and a current driving circuit, a rectangular electric pulse of 7.5 V is applied to the heater for $\sim 10\ \mu\text{s}$. The pulse is repeated periodically and

is controlled by the computer. In a typical measurement ~ 10 ballistic droplets are created per second and their motion is followed by video imaging.

We determined the droplet radius by weighing the cartridge before and after ejecting 9×10^4 droplets. The decrease in the cartridge mass was 6.5 ± 1 mg, averaged over several trials. This yields the average mass per droplet 72 ± 11 ng or a radius $R = 26 \pm 1$ μm . Independently, using fast video imaging, the terminal velocity $v_t = 7.6 \pm 1.1$ cm/s of the droplet was determined. For a small Reynolds number in air, $\text{Re}_a (\equiv 2Rv_t/\nu_a) < 1$, v_t of a sphere is approximately given by $v_t \simeq \frac{mg}{6\pi\eta_a R}$, where η_a and ν_a are respectively the shear and the kinematic viscosity of air. This yields a droplet radius of 25.4 ± 1.7 μm , which is in good agreement with the weighing method. In what follows, we will use $R_0 = 26$ μm as the radius of our droplets.

To study the interactions with a soap film, a stream of droplets generated by the inkjet nozzle is aimed normal to the film. For convenience of a latter discussion, a coordinate system is set up such that the initial velocity is along the x -axis and the film flows in \hat{y} direction as depicted in Fig. 1. The impact velocity v_i is varied by adjusting the distance between the nozzle and the film. After the collision, the droplet either tunnels through with a non-zero v_x or is absorbed by the film with $v_x = 0$. In this experiment, we measured the velocity components (v_x, v_y) after tunneling, as a function of the film thickness h and v_i . To visualize the droplet's trajectory, a high-intensity (300 W) halogen lamp and a high-speed video camera (Phantom V5, Vision Research) were used. The camera operates at several thousand frames per second, allowing droplet velocity to be measured reliably.

To determine the film thickness h , we measured the optical transmittance of the p -polarized light T_\perp at $\lambda = 685$ nm as a function of incident angle θ of a semiconductor laser. A rotation stage was built to allow the laser and a photodiode to be rotated synchronously on two separate arms. A computer controlled stepping motor drives the rotation stage, allowing a wide range of incident angle to be scanned rapidly, i.e., $-70^\circ \leq \theta \leq +70^\circ$ in ~ 5 s. We modeled the soap film as a dielectric slab of thickness h with a refractive index $n = 1.33$. A calculation shows that T_\perp is given by [15]

$$T_\perp = \left[1 + \left(\frac{2r_\perp}{1 - r_\perp^2} \right)^2 \sin^2(\delta/2) \right]^{-1}, \quad (1)$$

where $r_\perp = \frac{\cos \theta - \sqrt{n^2 - \sin^2 \theta}}{\cos \theta + \sqrt{n^2 - \sin^2 \theta}}$ and $\delta = \frac{4\pi h}{\lambda} \sqrt{n^2 - \sin^2 \theta}$. As shown in Fig. 2, this slab model

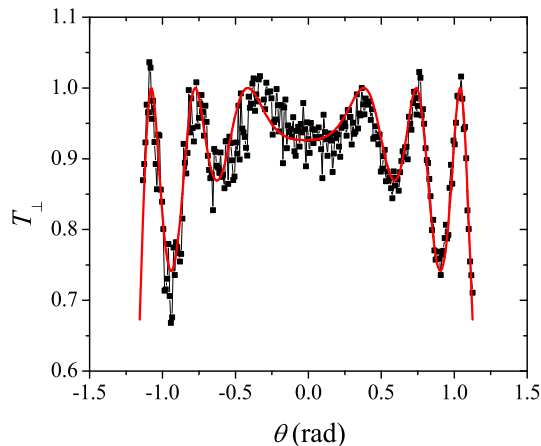


Figure 2: A typical optical transmission measurement in a flowing film. The data (dots) show transmittance T_{\perp} as a function of the incident angle θ . We found that a soap film can be well approximated by a dielectric slab with a constant thickness h and a refractive index $n = 1.33$. This allows T_{\perp} to be calculated rigorously. The solid line is a fit to the slab model of Eq. (1), resulting in $h \simeq 2.56 \mu\text{m}$ in this case.

works quite well for our soap films, and h can be accurately determined.

III. RESULTS AND DISCUSSIONS

Figure 3(a) displays the horizontal velocity component of the droplets after the impact on a soap film v_x as a function of v_i . The measurements were repeated for films of different thicknesses h . It is shown that there exists a critical velocity v_C ; for $v_i < v_C$, the droplet loses its horizontal momentum ($v_x = 0$) and it flows with the soap film after impact. On the other hand, for $v_i > v_C$, the droplet is able to tunnel through the film with $v_x > 0$. Although the data near the threshold is somewhat noisy, the critical velocity v_C can be determined without much ambiguity by extrapolating the data below and above the threshold. As delineated in the inset of Fig. 4, our measurements indicate that v_C increases with h , suggesting that the energy barrier for tunneling becomes greater for a larger h . We also found that v_C does not vanish when $h \rightarrow 0$ but approaches a finite value $v_{C0} \sim 520 \text{ cm/s}$, which translates to a minimum energy $E_{min}(\equiv \frac{1}{2}mv_{C0}^2) \simeq 0.01 \text{ erg}$. This suggests that a considerable fraction of the tunneling energy E_C is in the deformation of the soap film. Another conspicuous feature

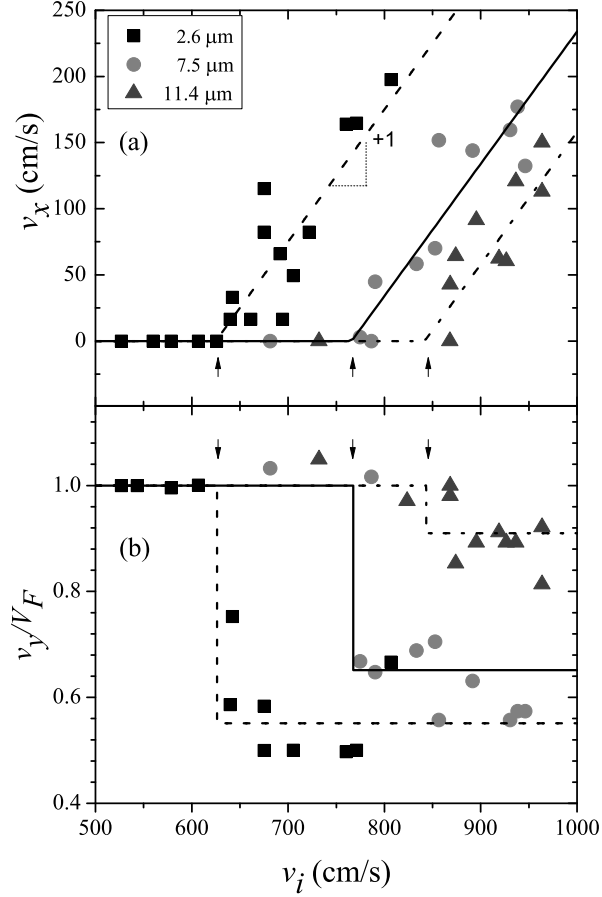


Figure 3: The droplet velocity (v_x, v_y) after impact as a function of the impact velocity v_i . The measurements were carried out for different film thicknesses: $h = 2.6 \mu\text{m}$ (squares), $7.5 \mu\text{m}$ (circles), and $11.4 \mu\text{m}$ (triangles). In (a), the x -component of the velocity v_x is plotted against v_i . It is shown that there exists a critical velocity v_C for each film thickness as indicated by the vertical arrows. In (b), the normalized y -component of the velocity v_y/V_F is plotted against v_i . Here we found that v_y/V_F has two discrete values for a given h . It is either $+1$ when the droplet merges with the film, or $\epsilon \leq 1$ when the droplet tunnels through the film.

seen in Fig. 3(a) is that after tunneling, v_x is linearly proportional to the impact velocity v_i , and the proportionality constant is to a good approximation unity for all different h .

In addition to the linear momentum exchange between the droplet and the soap film in the horizontal direction, the momentum exchange in the vertical direction is equally

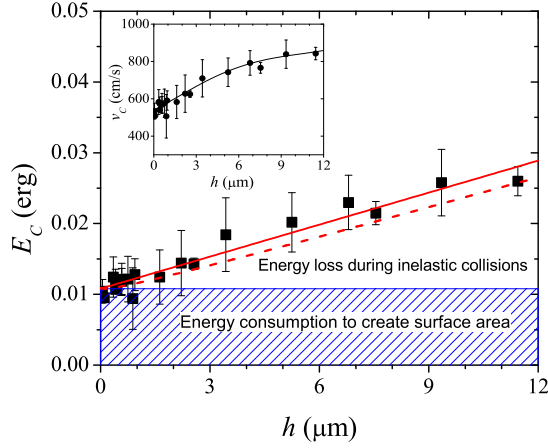


Figure 4: The critical velocity v_C and the energy barrier $E_C \equiv \frac{1}{2}mv_C^2$ vs. the film thickness h . In the inset, the critical velocity v_C is plotted against h . The solid line is a guide to the eyes. We define $E_C = \frac{1}{2}mv_C^2$, which is plotted as solid squares in the main graph. It is shown that $E_C(h)$ is approximately linear in h , but it does not vanish as $h \rightarrow 0$, indicating that a finite film deformation energy is required for tunneling. The solid line is a calculation based on Eq. (10), and the dotted line is a calculation based on Eq. (9). (see text for more details). The data points with $h < 2\mu\text{m}$ were measured using static soap films ($V_F = 0$).

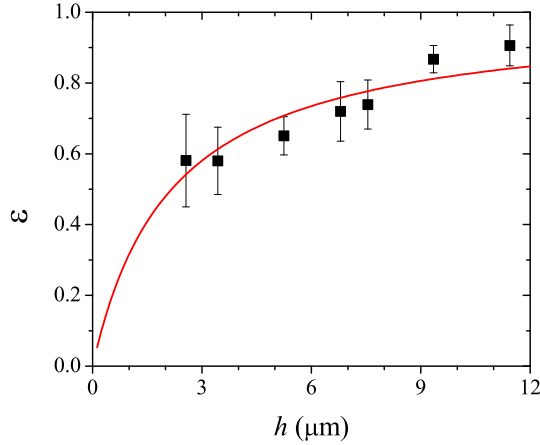


Figure 5: The normalized vertical velocity after tunneling $\epsilon = v_y/V_F$ vs. the film thickness h . It is observed that as h increases, ϵ becomes larger, indicating that the droplet gains a linear momentum in the \hat{y} direction. Asymptotically, $v_y \rightarrow V_F$ (or $\epsilon \rightarrow 1$) as $h \rightarrow \infty$ as expected. The solid line is a calculation based on Eq. (11) derived from an inelastic collision model.

significant. Fig. 3(b) displays normalized y -component velocity v_y/V_F as a function of the impact velocity v_i . It is shown that if $v_i < v_C$, $v_y/V_F = 1$, i.e. the droplet moves with the film. However, for $v_i > v_C$, the tunneling causes the droplet to gain a momentum in the \hat{y} direction, but in general $v_y < V_F$. Parameterizing the change in the y -component velocity of the droplet before and after tunneling $\epsilon = v_y/V_F$, we found that ϵ is nearly independent of v_i but it depends on the film thickness h as delineated in Fig. 5. It shows that when the droplet passes through a thicker film, it gains more momentum in the \hat{y} direction than passing through a thin one. Asymptotically, one expects that $\epsilon \rightarrow 1$ as $h \rightarrow \infty$, which is consistent with our observation. We found that a tunneling droplet readily picks up the y -momentum from the film. For instance, at the current experimental condition, v_y is $\sim 60\%$ of V_F for a film as thin as a few microns and is $\sim 90\%$ for $h \simeq 10 \mu\text{m}$.

To understand the physical origin of the energy barrier in the tunneling process, we examined carefully the impact dynamics using fast video imaging while the film was illuminated by a monochromatic sodium lamp. Fig. 6 (a-d) displays four consecutive images of a droplet shortly after it had impacted on a soap film of thickness $h = 4 \mu\text{m}$. The time interval between the images was fixed at 0.26 ms. Here, the droplet as well as its mirror image on the soap film are clearly visible. Also visible in (b) is a scar created by the droplet, but the scar disappeared in (c), indicating that its lifetime is less than 0.26 ms. Because of the short length and time scales involved, we believe that the scar region is associated with strong vorticity, which dissipates energy. The use of the monochromatic light also allowed us to observe waves created by the impact. Here, the wavefront appears as a dark band in (b) that propagates radially outward. In Fig. 7(a-d), another sequence of images is captured at an equal interval 0.2 ms by setting the camera normal to the surface of the soap film. Here the droplet is merged with the film because it impacts the film at the velocity lower than v_C . The merging droplet is visible as a dark spot at the center of the circular wavefront and is carried downstream by the film. As it moves downstream, the wavefront propagates radially outward at a constant velocity v_w . By investigating images such as ones in Fig. 7, the wave speed v_w on the soap film can be determined as a function of h , which is displayed as solid squares in Fig. 7(e). The figure shows that v_w increases rapidly as h decreases; for a small thickness, $h < 1 \mu\text{m}$, v_w can be as large as 10 m/s. A liquid film in general can support two different types of waves, known as the symmetric and the anti-symmetric waves [16]. For the symmetric wave, the two surfaces of the film move out of

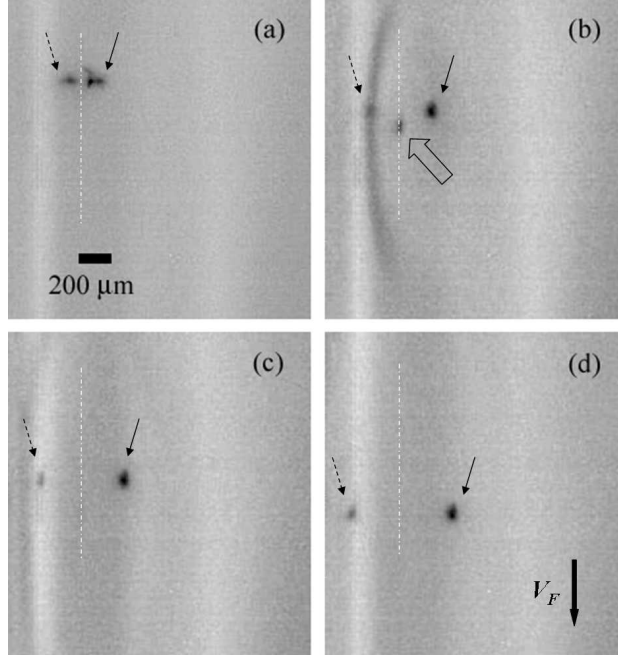


Figure 6: The tunneling dynamics of a water droplet. The sequence of video images (a-d) were taken at an equal time interval with $t = 0, 0.26, 0.52$, and 0.78 ms. Here the penetrating droplet and its mirror image are clearly visible and are marked by the pair of arrows, where the dotted lines depict the plane of reflection. As a function of time, the droplet/image pair moves together in the vertical direction, but they moves apart from each other in the horizontal direction. This allows a precise determination of v_x and v_y . Shortly after the impact, an elongated dark region can be identified in (a), showing that the film is stretched by the droplet. A moment later (b), a scar, which is indicated by a large arrow, is left behind in the film. The scar moves with V_F , which is faster than the droplet velocity v_y . This yields a precise determination of the velocity difference $v_y - V_F$ or ϵ . Interestingly, the scar in (b) disappears rapidly and is no longer observable in (c). Also seen in (b) is the surface wave (the dark band) that propagates radially outwards from the impact point.

phase with respect to each other, and is also called peristaltic mode of oscillations (see Fig. 8(b)). For the anti-symmetric wave, both surfaces undulate in phase (see Fig. 8(c)). In the absence of surfactants, the restoring force of both waves are due to the surface tension σ but the dispersion relations are different for the two cases because of different mass distributions in the film. The anti-symmetric wave is non-dispersive with a constant velocity given by $v_a = \sqrt{\frac{2\sigma}{\rho_w h}}$, and the symmetric wave, on the other hand, is dispersive with a velocity

$v_s = k\sqrt{\frac{\sigma h}{2\rho_w}}$ that depends on a wavenumber k . Since $v_s/v_a = kh/2$, it is expected that $v_a \gg v_s$ in the long-wavelength limit. In the presence of surfactants, the restoring force for the peristaltic mode is dominated by the surface (or Marangoni) elasticity $E \equiv A\frac{d\sigma}{dA}$, where A is a surface area, instead of σ . It is shown by Lucassen [17] that in the long-wavelength limit, the elastic wave is also non-dispersive with a propagation speed $v_e = \sqrt{\frac{2E}{\rho_w h}}$. In our soap film therefore there is a degeneracy in that both the anti-symmetric capillary wave and the symmetric elastic wave are possible, and both scale with the film thickness as $h^{-1/2}$. We found that our experimental data in Fig. 7 can be well described by the mathematical form $v_w = \sqrt{\frac{2c}{\rho_w h}}$ (see the inset), where c is an adjustable parameter. Using $\rho_w = 1 \text{ g/cm}^3$, a fitting procedure yields $c \simeq 32.7 \pm 2.6 \text{ erg/cm}^2$, which matches very well with the surface tension measurement ($\sigma = 32 \text{ erg/cm}^2$) using the Du Noüy ring method. Thus, unless it is an amazing coincidence, where Marangoni elasticity E is nearly identical to σ for our soap film, we believe that the dominant wave mode in the film created by the droplet impact is the anti-symmetric wave.

At the impact point (see Fig. 6(a)), it is observed that the droplet deforms the soap film locally, forming a cylindrical pouch a few droplet diameters long. Because of smallness of the droplet and fast dynamics, it was not feasible to follow the spatiotemporal evolution of the cylindrical pouch. However, inspections of a large number of video images reveal that the longest pouch is $\sim 4R_0$, indicating that in order to tunnel through, the soap film must be stretched into a long cylinder with an excess surface area of $\sim 14\pi R_0^2$, where R_0 is the radius of the water droplets. A naive calculation using $\sigma = 32 \text{ erg/cm}^2$ indicates that this corresponds to a surface energy of $9.5 \times 10^{-3} \text{ erg}$. Considering the Marangoni effect, we expect that the energy requirement may be greater.

A question that arises naturally is what determines the maximum length of the cylinder. A related phenomenon is the Plateau-Rayleigh instability where a uniform circular jet of fluid breaks up into a stream of droplets [18]. For the anti-symmetric undulation to be the dominant mode of oscillations in our soap film, the instability of a cylindrical soap film is similar to the Plateau-Rayleigh problem with the simple modification of replacing the surface tension σ by 2σ , due to the presence of two liquid-air interfaces of the film. It follows that the fastest growing wavenumber k_{max} of the axial undulation is given by $k_{max} \simeq 0.7/R_0$, corresponding to $\lambda_{max}(\equiv 2\pi/k_{max}) \simeq 9R_0$ [18]. We note that our experimentally observed pouch length $4R_0$ is about a half of λ_{max} , which makes physical sense since the front of

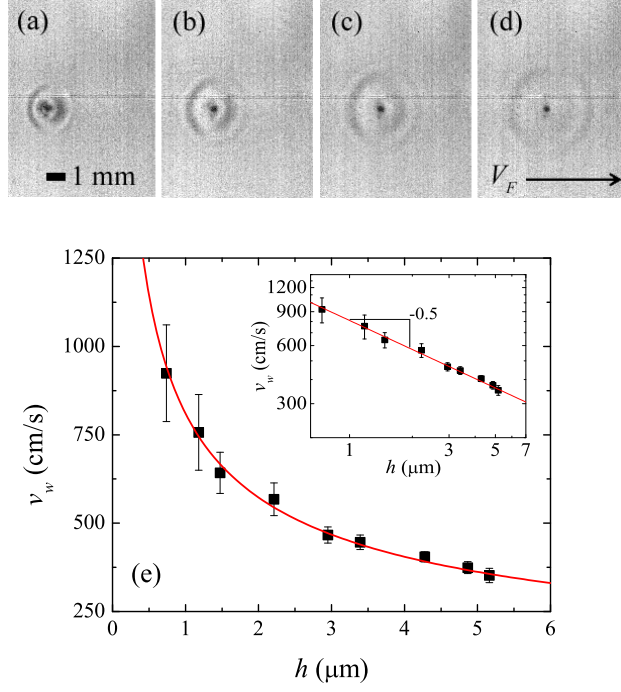


Figure 7: A wave generated by an impacting droplet. Images (a-d) were taken sequentially at an equal interval, corresponding to $t = 0, 0.2, 0.4$, and 0.6 ms, respectively. The impact velocity of the droplet is less than v_C so that it merges with the soap film. The droplet appears as a dark spot at the center of the expanding circular wavefront. In (e), the wave speed v_w in the soap films is measured as a function of h . The scaling relation $v_w \propto h^{-1/2}$ is delineated in the inset, where the solid line is a fit to $v_w = \sqrt{\frac{2\sigma}{\rho_w h}}$.

the pouch, where the water droplet locates, must be the anti-node and the location of the pinch-off must be the node given by $(n + \frac{1}{2})\lambda_{max}$ where $n = 0, 1, 2, \dots$. Our observation corresponds to $n = 0$ (see Fig. 8(a)). This is possible if the pinch-off time τ is shorter than the stretching time ($\sim \lambda_{max}/2U$), because otherwise a longer pouch will be produced and it will break in multiple locations, which was not observed. Quantitatively, this scenario also makes sense since according to our measurement the stretching time is $\lambda_{max}/2U \simeq 12 \mu s$ and the pinch-off time τ can be estimated by the growth rate of the Plateau-Rayleigh instability $\tau \equiv \sqrt{\rho_a R_0^3 / 2\sigma} \simeq 0.52 \mu s$. Thus the condition $\tau \ll \lambda_{max}/2U$ is satisfied. The emerging physical picture is that during transmission, a piece of soap film is extruded by the fast moving droplet. At the same time an axial undulation grows rapidly on the stretched cylindrical film, and the cylinder closes off at its base once $\lambda_{max}/2$ is reached. As we will

show below, in order to explain the kinematics of the tunneling droplet, a small mass must be transferred from the film to the droplet and the size of such a mass can be determined from our measurements.

IV. CALCULATIONS

It would be desirable to compare our experimental observations with theoretical predictions. Unfortunately such theory is not currently available. A back-of-the-envelope calculation shows that our measurements were carried out in a hydrodynamic regime where Reynolds number $\text{Re} = \frac{2\rho_w R_0 v_i}{\eta_w} \gtrsim 260$ and the Weber number $\text{We} = \frac{2\rho_w R_0 v_i^2}{\sigma} \gtrsim 44$ are both large. Thus the kinetic energy or the inertia effect overwhelms energy dissipation and the capillary effect. In the following we propose a heuristic model that can account for some key features of our observations.

It is apparent that when a collision takes place, only a fraction of film mass in the neighborhood of the impact is involved in the interaction. Thus an effective mass M_1 and its corresponding size $R_1 = \sqrt{M_1/\pi\rho_w h}$ may be specified. After the collision, a part of M_1 , called M_2 , is transferred to the water droplet, increasing its mass from m to $m + M_2$. The emerging droplet travels with velocity (v_x, v_y) and the remaining mass $M_1 - M_2$ travels along the film with velocity (v'_x, v'_y) (see Fig. 8(a)). The presence of M_2 allows a second length scale $R_2 = \sqrt{M_2/\pi\rho_w h}$ to be specified. We treat our problem as an inelastic collision in which linear momentum is conserved but not energy.

The linear momentum conservation demands

$$mv_i = (m + M_2)v_x + (M_1 - M_2)v'_x, \quad (2)$$

$$M_1 V_F = (m + M_2)v_y + (M_1 - M_2)v'_y. \quad (3)$$

At the moment of separation, when the dressed droplet $(m + M_2)$ becomes detached from the rest of the film, we expect that $v_x > 0$ but $v'_x \simeq 0$. For the inelastic collision, one also expects $v_y = v'_y$ at the separation point. Solving the above equations, we find

$$v_x = \frac{m}{m + M_2} v_i, \quad (4)$$

$$v_y = v'_y = \frac{M_1}{m + M_1} V_F. \quad (5)$$

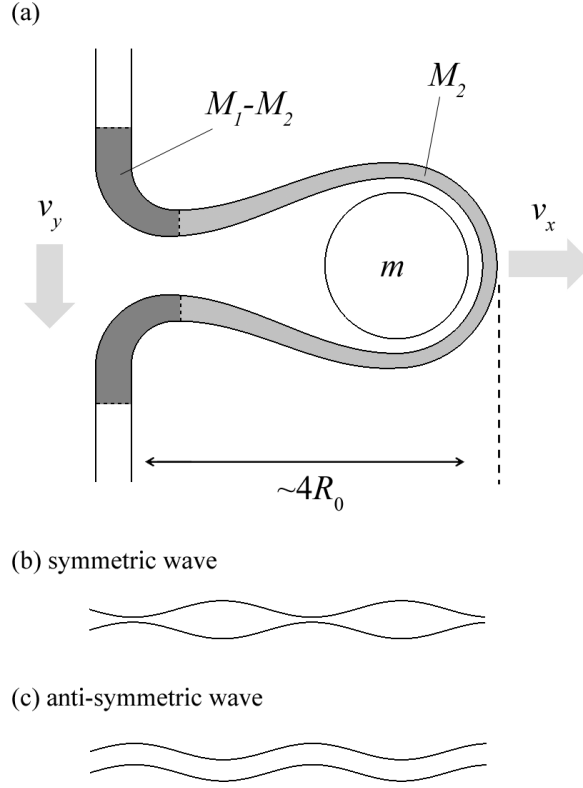


Figure 8: The schematics depicting different conformations of a soap film. In (a), the film is stretched by a ballistic droplet, where M_2 will eventually engulf droplet m , and M_1 provides a y -momentum to the droplet. (b) and (c) are two possible wave modes in a soap film.

The total kinetic energy KE_f of the droplet and the film after collision is given by

$$\begin{aligned}
 KE_f &= \frac{1}{2}(m + M_2)(v_x^2 + v_y^2) + \frac{1}{2}(M_1 - M_2)(v_y'^2), \\
 &= \frac{1}{2} \frac{m}{m + M_2} m v_i^2 + \frac{1}{2} \frac{M_1}{m + M_1} M_1 V_F^2.
 \end{aligned} \tag{6}$$

Neglecting the deformation of the film, this is all the mechanical energy of the system (droplet plus the soap film) that remains after the collision. It is clear that the collision is inelastic since

$$\begin{aligned}
 \Delta KE &(\equiv KE_i - KE_f) \\
 &= \frac{1}{2} m \left(\frac{M_2}{m + M_2} v_i^2 + \frac{M_1}{m + M_1} V_F^2 \right) \geq 0,
 \end{aligned} \tag{7}$$

where $KE_i = \frac{1}{2}mv_i^2 + \frac{1}{2}M_1V_F^2$ is the total kinetic energy of the system before the collision. Physically, ΔKE is the amount of energy ultimately dissipated by the creation of vorticity in the fluid. Since both M_1 and M_2 are proportional to h , we found that energy dissipation vanished when $h \rightarrow 0$. In other words, no vorticity can be created in a very thin film so the physics of tunneling becomes a purely potential flow problem. For a successful transmission, the energy consideration therefore requires that the initial energy of the droplet should be greater than the sum of the energy dissipation ΔKE and the film deformation E_{min} with the result: $KE_i \geq \Delta KE + E_{min}$ (or $KE_f \geq E_{min}$). This yields

$$\frac{1}{2}mv_i^2 \geq E_{min} \left(1 + \frac{M_2}{m}\right) - \frac{1}{2}mV_F^2 \left(\frac{m + M_2}{m + M_1}\right), \quad (8)$$

or the critical energy of the droplet $E_C = \frac{1}{2}mv_C^2$ as:

$$E_C = E_{min} \left(1 + \frac{M_2}{m}\right) - \frac{1}{2}mV_F^2 \left(\frac{m + M_2}{m + M_1}\right). \quad (9)$$

This equation correctly predicts that the motion of the film ($V_F \neq 0$) lowers the energy barrier of tunneling. For a small V_F , e.g., in our experiment $(V_F/v_C)^2 < 0.15$, one may neglect the last term to obtain,

$$E_C \simeq E_{min} \left(1 + \frac{M_2}{m}\right) = E_{min} \left(1 + \frac{3}{4}\alpha_2^2 \frac{h}{R_0}\right), \quad (10)$$

where $\alpha_2 = R_2/R_0$ is a constant. Eq. (10) is consistent with our observation in that E_C is linear in h with a finite intercept (see Fig. 4). Using the known parameters of our soap film ($E_{min} \simeq 0.01$ erg and $R_0 = 26 \mu\text{m}$), we found $\alpha_2 \simeq 2.2 \pm 0.1$. Interestingly, this value of α_2 implies a rather uniform coating of the penetrating droplet by the film of thickness h , i.e., $\Delta V \simeq 4\pi R_0^2 h$. In Fig. 4 we showed that Eq. (10) (solid line) and Eq. (9) (dotted line) both agree reasonably with our measurements.

According to Eq. (5), the emerging droplet will have a velocity in vertical direction

$$v_y = \frac{M_1}{m + M_1} V_F = \frac{V_F}{1 + \frac{4}{3} \left(\frac{R_0}{\alpha_1^2 h}\right)}, \quad (11)$$

where $\alpha_1 = R_1/R_0$. This equation yields the correct asymptotic behavior, $\epsilon(h)(\equiv v_y/V_F) \rightarrow 1$ as $h \rightarrow \infty$, as seen in Fig. 5. Using α_1 as an adjustable parameter, a fitting procedure gives $\alpha_1 \simeq 4.0 \pm 0.4$, which is delineated by the solid line in Fig. 5.

V. CONCLUSION

Using well-controlled micron-sized ballistic droplets generated by an inkjet cartridge, we have characterized the energy requirement for tunneling of these droplets through a flowing soap film. The energy barrier $E_C(h)$ is found to be linearly proportional to the film thickness h with the result: $E_C = E_{min}(1 + \alpha h/R_0)$. Here the minimal barrier height $E_{min}(\equiv \frac{1}{2}mv_{C0}^2) \simeq 0.01 \text{ erg}$ and the slope $\alpha = 3.9$ are determined. The measured E_{min} corresponds to the creation of an excess surface area of $\sim 14\pi R_0^2$, which turns out to be consistent with the Rayleigh instability condition of pinching off at $\lambda_{max}/2$. The observed E_{min} also implies the existence of a critical Weber number $We_C(\equiv 2\rho_w R_0 v_{C0}^2/\sigma) \simeq 44$, when the film inertia is unimportant, $h \rightarrow 0$.

A self consistent theory is not currently available, and we wish that our observations will provide a useful foundation for such theory. The dynamics is clearly complex in that it involves multiple length and time scales. We have identified two such scales, R_1 and R_2 , that are needed to account for the energy and momentum exchanges between the droplet and the film. A self consistent theory must deal with additional length scales, corresponding to early-time or short-length-scale events, where Re is small, and vorticity production, hence energy dissipation, is prominent. The physics in this regime may explain the intriguing observation that the energy dissipation becomes negligible for some macroscopically thin but microscopically thick films; i.e., the limit $h \rightarrow 0$ must correspond to a film that is still thick enough so that it can be stretched to the Rayleigh instability limit. Another issue of interest is the separation dynamics of a tunneling droplet from the rest of the film. This is a singular event that produces discontinuities, such as $v_x \neq v'_x$ at the moment of separation.

This investigation was initially motivated by our desire to print ink patterns in a turbulent flowing soap film and to study how different spatial modes of the pattern are dispersed by turbulent eddies. This would allow passive-scalar turbulence to be studied in a controllable fashion with a defined initial condition. Our measurements presented above give a parameter range for ink droplets to remain on the surface of a moving film, which is a prerequisite for a successful conduct of such measurement. We also found that a ballistic water droplet is an effective wave generator; we had no difficulty of observing the anti-symmetric waves in the film and were able to precisely determine their speeds for different film thicknesses. Curiously, however, the symmetric waves remain elusive. Unlike anti-symmetric waves, the

symmetric wave is an important attribute of a soap film and would allow experimenters to obtain useful information about Marangoni elasticity, which is not readily measured in a film. The failure to observe such a wave suggests that the peristaltic oscillations must decay fast and hence not be detectable in our current experimental setting. We wish to examine this issue more carefully in future experiments.

Aside from its academic interest, the ability of small particles to penetrate a fluid film without damaging it can have important technological applications such as encapsulation of solid particles and transmission of genetic materials through biological cells. The latter is a fascinating application of ballistic transmission in biological systems where gold particles coated with DNA molecules of interest can be delivered into plant or animal cells [19]. A better understanding of transmission kinematics, such as the one studied here, may shed new light on its working principle and can ultimately improve the quality of this important technology.

VI. ACKNOWLEDGMENT

This work is supported by the NSF under the grant no. DMR-0242284.

-
- [1] H. E. Edgerton and J. R. Killian, *Flash!* (Branford Boston, 1939).
 - [2] S. T. Thoroddsen, J. Fluid Mech. **451**, 373 (2002).
 - [3] C. Josserand and S. Zaleski, Phys. Fluids **15**, 1650 (2003).
 - [4] L. Xu, W. Zhang, and S. Nagel, Phys. Rev. Lett. **94**, 184505 (1995).
 - [5] D. A. Weiss and A. L. Yarin, J. Fluid Mech. **385**, 229 (1999).
 - [6] G. I. Taylor and D. H. Michael, J. Fluid Mech. **58**, 625 (1973).
 - [7] R. Zheng and T. A. Witten, Phys. Rev. E **74**, 051602 (2006).
 - [8] Y. Couder, J. Phys. Lett. Paris **45**, 353 (1984).
 - [9] B. K. Martin, X. L. Wu, and W. I. Goldburg, Phys. Rev. Lett. **80**, 3964 (1998).
 - [10] P. Vorobieff, M. Rivera, and R. E. Ecke, Phys. Fluids **11**, 2167 (1999).
 - [11] N. Y. Liang, C. K. Chan, and H. J. Choi, Phys. Rev. E **54**, R3117 (1996).
 - [12] L. Courbin and H. A. Stone, Phys. Fluids **18**, 091105 (2006).

- [13] M. A. Rutgers, X. L. Wu, R. Bhagavatula, A. A. Petersen, and W. I. Goldburg, *Phys. Fluids* **8**, 2847 (1996).
- [14] X. L. Wu, R. Levine, M. Rutgers, H. Kellay, and W. I. Goldburg, *Rev. Sci. Instrum.* **72**, 3025 (2001).
- [15] E. Hecht, *Optics* (Addison Wesley, 1998), 3rd ed.
- [16] G. I. Taylor, *Proc. R. Soc. Lond. A* **253**, 296 (1959).
- [17] J. Lucassen, M. V. den Tempel, A. Vrij, and F. Hesselink, *Proc. K. Ned. Akad. Wet. B* **73**, 109, 124 (1970).
- [18] S. Chandrasekhar, *Hydrodynamics and Hydromagnetic Stability* (Dover, 1981).
- [19] M. T. S. Lin, L. Pulkkinen, J. Uitto, and K. Yoon, *Int. J. Dermatol.* **39**, 161 (2000).